Combined Geometric and Neural Network Approach to Generic Fault Diagnosis in Satellite Reaction Wheels

Baldi, P.; Blanke, Mogens; Castaldi, P.; Mimmo, N.; Simani, S.

Published in:
I F A C Workshop Series

Link to article, DOI:
10.1016/j.ifacol.2015.09.527

Publication date:
2015

Document Version
Peer reviewed version

Combined Geometric and Neural Network Approach to Generic Fault Diagnosis in Satellite Reaction Wheels

P. Baldi [*,1] **M. Blanke** [**] **P. Castaldi** [*] **N. Mimmo** [*]
S. Simani [***]

[*] *Department of Electrical, Electronic and Information Engineering, University of Bologna, Faculty of Aerospace Engineering. 47100 Forlì(FC), ITALY. (e–mail: pietro.baldi@studio.unibo.it).*
[**] *Automation and Control Group, Department of Electrical Engineering, Technical University of Denmark, 2800 Kgs. Lyngby, DENMARK. (e–mail: mb@elektro.dtu.dk)*
[***] *Department of Engineering, University of Ferrara. 44123 Ferrara (FE), ITALY. (e–mail: silvio.simani@unife.it).*

Abstract: This paper suggests a novel diagnosis scheme for detection, isolation and estimation of faults affecting satellite reaction wheels. Both spin rate measurements and actuation torque defects are dealt with. The proposed system consists of a fault detection and isolation module composed by a bank of residual filters organized in a generalized scheme, followed by a fault estimation module consisting of a bank of adaptive estimation filters. The residuals are decoupled from aerodynamic disturbances thanks to the Nonlinear Geometric Approach. The use of Radial Basis Function Neural Networks is shown to allow design of generalized fault estimation filters, which do not need a priori information about the faults internal model. Simulation results with a detailed nonlinear spacecraft model, which includes disturbances, show that the proposed diagnosis scheme can deal with faults affecting both reaction wheel torques and flywheel spin rate measurements, and obtain precise fault isolation as well as accurate fault estimates.

Keywords: Fault diagnosis, geometric approaches, neural networks, actuators, sensors, satellite control applications.

1. INTRODUCTION

The increasing requirements for onboard autonomy in satellite control systems cause a need for methods that support design of complete and reliable supervisory systems. An essential feature in demand is the accurate diagnosis of potential faults, and subsequent fault accommodation actions to improve system reliability and availability. In this context, Fault Detection and Diagnosis (FDD) systems provide fundamental information about the health status of the system jointly with the estimation of the occurred faults.

Significant research in FDD has been done in last three decades (Blanke et al. (2006); Isermann (2006)). Numerous model-based methods have been proposed for fault diagnosis (Ding (2008)). Many techniques are based on linear models, which may be affected by significant modelling errors. Several approaches have also been proposed for nonlinear systems (Bokor and Szabó (2009); Edelmayer et al. (2004)). The work presented by De Persis and Isidori (2001) provides a solution to the Fault Detection and Isolation (FDI) problem for nonlinear systems by using a NonLinear Geometric Approach (NLGA). Several methods have been proposed for the diagnosis of faults affecting satellite reaction wheels (Lorentzen et al. (2003); Sobhani–Tehrani et al. (2014)).

This paper suggests a novel diagnosis scheme for detection, isolation and estimation of faults affecting both the spin rate measurements (*i.e.* sensor faults) and the actuated torques (*i.e.* actuator faults) of satellite reaction wheels. The procedure for actuator and sensor fault modeling presented by Mattone and De Luca (2006) is exploited to define a nonlinear model affine in all the actuator and sensor fault inputs, a model structure suitable for the use of the NLGA.

The performance of the proposed FDD system is evaluated on a detailed nonlinear satellite simulator taking account also of exogenous disturbance signals. The FDD robustness is achieved by exploiting an explicit disturbance decoupling method, based on the NLGA, applied to the aerodynamic force term, which represents the main source of uncertainty in the satellite dynamic model (Baldi et al. (2013)). The approach in this paper is to design a model-based FDD system composed by an FDI module consisting of a bank of scalar residual filters and a fault estimation module consisting of a bank of scalar adaptive estimation filters. The residual filters are designed via the NLGA (De Persis and Isidori (2001)). The use of the NLGA allows to obtain residual filters and diagnostic signals that are independent of the aerodynamic disturbance parameters. The fault isolation task is achieved, with the

[1] Corresponding author.

assumption of multiple nonconcurrent faults, through the use of a residual cross-check and a decision logic.
The adaptive estimation filters are designed via the NLGA and a Radial Basis Function Neural Network (RBF NN) (Castaldi et al. (2014)). The estimation module is activated once a fault is correctly detected and isolated by the FDI module. The designed adaptive filters provide accurate fault estimates, which are independent of the aerodynamic disturbance and satellite attitude. The joint use of these two methods allows to take advantage of the benefits of both. The use of a RBF NN allows to design *generalised fault estimation filters* which do not need a priori information about the fault type. Thus, the FDD adaptive filters can estimate a generic fault without needing to define any specific fault internal model. Moreover, the NLGA allows to obtain accurate fault estimates without errors due to parameter uncertainties.

2. SPACECRAFT AND ACTUATOR MODELS

The spacecraft is considered as a rigid body, whose attitude is represented by using the quaternion notation. The satellite mathematical model is given by the dynamic and kinematic equations of (1) and (2) (Wie (2008)), where $\omega = [\omega_1, \omega_2, \omega_3]^T$ is the vector of body rates in roll, pitch, and yaw, respectively, whilst $\mathbf{q} = [q_1, q_2, q_3, q_4]^T$ is the quaternion vector and $\mathbf{h}_w$ is the vector of the flywheel angular momenta. The principal inertia body-fixed frame is considered, with I_{xx}, I_{yy}, and I_{zz} the elements on the main diagonal of the satellite inertia matrix $\mathbf{I}_s$.

$$\dot{\omega} = -\mathbf{I}_s^{-1}\mathbf{S}(\omega)(\mathbf{I}_s\omega + \mathbf{h}_w) + \mathbf{I}_s^{-1}(\mathbf{M} + \mathbf{M}_{gg} + \mathbf{M}_{aero}) \quad (1)$$

$$\dot{\mathbf{q}} = \frac{1}{2}\mathbf{\Omega}\mathbf{q} \quad (2)$$

with the skew-symmetric matrices

$$\mathbf{S}(\omega) = \begin{bmatrix} 0 & -\omega_3 & \omega_2 \\ \omega_3 & 0 & -\omega_1 \\ -\omega_2 & \omega_1 & 0 \end{bmatrix}, \mathbf{\Omega}(\omega) = \begin{bmatrix} 0 & \omega_3 & -\omega_2 & \omega_1 \\ -\omega_3 & 0 & \omega_1 & \omega_2 \\ \omega_2 & -\omega_1 & 0 & \omega_3 \\ -\omega_1 & -\omega_2 & -\omega_3 & 0 \end{bmatrix} \quad (3)$$

The dynamic equations explicitly include the models of the gravitational and aerodynamic disturbance torques $\mathbf{M}_{gg}$ and $\mathbf{M}_{aero}$ about the centre of mass and described in the body-fixed frame. Both the disturbances are dependant on the satellite attitude. These disturbances typically represent the most important external disturbance torques affecting Low Earth Orbit (LEO) satellites (Wie (2008)). The design of the FDI system exploits an explicit decoupling only of the aerodynamic torque since the gravitational disturbance has a model which is *almost perfectly known*, and thus its effect does not need to be decoupled. Regarding the gravity gradient torque $\mathbf{M}_{gg}$, the parameters μ and R in (4) represent the gravitational constant and the orbit radius respectively, R is the satellite distance from the Earth center and $\hat{v}_{nadir}$ is the unit vector towards nadir expressed in body-frame coordinates.

$$\mathbf{M}_{gg} = \frac{3\mu}{R^3}(\hat{v}_{nadir} \times I_s\hat{v}_{nadir}) \quad (4)$$

Regarding the aerodynamic torque $\mathbf{M}_{aero}$, it depends on the aerodynamic force represented in (5) by the relation $F_{aero} = \frac{1}{2}\rho S_p V^2 C_D$, where ρ is the atmospheric density, V is the relative velocity of the satellite, S_p is the reference area affected by the aerodynamic flux, and C_D is the drag coefficient. $\mathbf{r_{cp}} = \left[r_{x_{cp}}, r_{y_{cp}}, r_{z_{cp}}\right]^T$ is the vector joining the centre of mass and the aerodynamic centre of pressure and $\hat{v}_V$ is the unit velocity vector expressed in body-frame coordinates. It is worth noting that, mainly due to the presence of the unknown terms ρ and C_D, the input signal $\mathbf{M}_{aero}$ in (1) represents the main source of uncertainty. Therefore, residual generators and adaptive estimation filters need to be independent of the aerodynamic disturbance. The aerodynamic torque is

$$\mathbf{M}_{aero} = \frac{1}{2}\rho S_p V^2 C_D(\hat{v}_V \times \mathbf{r}_{cp}) \quad (5)$$

The dynamic equations include also the gyroscopic terms due to cross-couplings between the satellite angular rates and flywheel spin rates. In order to perform an optimized attitude and manoeuvre control, a control law including also a compensation term have been implemented to compensate for this gyroscopic cross-coupling due to high system momentum conditions, represented by the first term of (1) (Calhoun and Garrick (2007)). It is worth observing that, since these compensation terms are derived by exploiting also spin rate measurements provided by the reaction wheel sensors, accurate measurements are required and possible sensor faults needs to be accurately detected, isolated and estimated to allow following fault accommodation actions.
Finally, the considered satellite ACS consists of a fixed array of three reaction wheels aligned with respect to the principal axes of inertia. The elements of the control input vector $\mathbf{M} = [M_1, M_2, M_3]^T$ correspond to the attitude control torques actuated by the considered actuators with respect to their main rotation angles.
These control torques give also the rates of change of the angular momenta of the reaction wheels. The dynamic equations of the actuators are given in (6), where $\mathbf{h}_w = J_w\omega_w = [h_1, h_2, h_3]^T$ is the vector of the wheel angular momenta, $\omega_w = [\omega_{w_1}, \omega_{w_2}, \omega_{w_3}]^T$ is the vector of the reaction wheel spin rates and J_w denotes the flywheel inertia:

$$\dot{\omega}_w = {J_w}^{-1}\dot{\mathbf{h}}_w = -{J_w}^{-1}\mathbf{M} \quad (6)$$

The overall system model can be described by (1), (2) and (6). Thus, the overall state vector can be represented by $x = [\omega_1, \omega_2, \omega_3, q_1, q_2, q_3, q_4, \omega_{w_1}, \omega_{w_2}, \omega_{w_3}]^T$, and all the state variables are assumed to be measurable.

3. FAULT DETECTION AND ISOLATION

3.1 Nonlinear Geometric Approach

The NonLinear Geometric Approach (NLGA) was formally developed by De Persis and Isidori (2001), and it relies on a coordinate change in the state and output spaces providing an observable subsystem which, if it exists, is affected by the fault, but unaffected by disturbances and the other faults to be decoupled. The NLGA residual filters for FDI are designed by exploiting the properties of this subsystem. In particular, the approach considers

a nonlinear system model, affine in the control and fault inputs, in the form

$$\begin{cases} \dot{x} = n(x) + g(x)\, u_c + \ell(x)\, f + p(x)\, d \\ y = h(x) \end{cases} \tag{7}$$

in which the state vector $x \in \mathcal{X}$ (an open subset of $\mathcal{R}^{\ell_n}$), $u_c(t) \in \mathcal{R}^{\ell_u}$ is the commanded control input vector, $f(t) \in \mathcal{R}$ is the fault (or a subset of faults) to be detected, $d(t) \in \mathcal{R}^{\ell_d}$ the disturbance vector (embedding also all the faults to be decoupled), and $y \in \mathcal{R}^{\ell_m}$ the output vector. $n(x)$, $\ell(x)$, the columns of $g(x)$ and $p(x)$ are smooth vector fields, and $h(x)$ is a smooth map. Therefore, if P represents the distribution spanned by the column of $p(x)$, the NLGA method can be devised (De Persis and Isidori (2001)).
If $\ell(x) \notin (\Omega^*)^{\perp}$, where Ω^* denotes the largest observability codistribution contained in $P^{\perp}$, the fault results to be detectable. Whenever the previous fault detectability condition is satisfied, (local) diffeomorphisms can be found, which represent a coordinate change in the state and output spaces. Hence, in the new (local) coordinates, the system (7) can be decomposed into 3 subsystems (*i.e.* $\bar{x}_1$, $\bar{x}_2$ and $\bar{x}_3$), where $\bar{x}_1$ represents the measured part of the state which is affected by f and not affected by d, whilst $\bar{x}_2$ and $\bar{x}_3$ represent the measured and not measured part of the state, which are affected by f and d. In many cases $\bar{x}_3$ is not present. Denoting $\bar{x}_2$ with $\bar{y}_2$ and considering it as an independent input, the $\bar{x}_1$-subsystem, affected by the fault term f with $\ell_1(\bar{x}_1, \bar{y}_2, \bar{x}_3)$ not identically zero and decoupled from the disturbance term d, can be derived as

$$\begin{cases} \dot{\bar{x}}_1 = n_1(\bar{x}_1, \bar{y}_2) + g_1(\bar{x}_1, \bar{y}_2)\, u_c + \ell_1(\bar{x}_1, \bar{y}_2, \bar{x}_3)\, f \\ \bar{y}_1 = h(\bar{x}_1) \end{cases} \tag{8}$$

3.2 Aerodynamic Disturbance, Actuator and Sensor Fault Modeling

It is assumed that at most one fault can affect the system at any time (*non-concurency* of faults). Being (1) and (6) already affine in the control inputs, the i-th actuator fault can be simply modelled through the following fault input:

$$f_{M\,i} = M_i - M_{c,i}, (i = 1, ..., 3) \tag{9}$$

and corresponding vector field $\ell_{M_1}(x)$, where M_c represents the vector of the commanded control inputs.
Regarding the sensor faults, the most natural way to take into account their occurrence would be defining the j-th measurement fault

$$F_{\omega_j} = \omega_{w_j} - \omega_{w_{y,j}}, (j = 1, ..., 3) \tag{10}$$

as the difference between the real value ω_{w_j} and measured value $\omega_{w_{y,j}}$ of the j-th flywheel spin rate. However, this modeling would lead to the appearance of fault terms in the output equations, or more in general even to models nonlinear in the sensor fault inputs.
A different modeling procedure for sensor faults was proposed by Mattone and De Luca (2006) and hereby applied, which allows to obtain a dynamic model exploitable for the FDI design with the same structure affine in the fault inputs of (7). Essentially, the procedure consists in introducing a suitable set of $\nu_k \geq 1$ *mathematical* fault inputs $f_{\omega_{j,k}}$, $k = 1, ..., \nu_k$, in place of the *physical* sensor fault F_{ω_j}. Whenever a physical sensor fault $F_{\omega_j} \neq 0$ occurs, all the associated mathematical fault inputs $f_{\omega_{j,k}}$ will become generically nonzero, although with completely different time behaviors and, in general, without a direct physical interpretation. Hence, in order to detect and isolate the occurrence of a single physical sensor fault, it will be sufficient to recognize the occurrence of *any* (one or more) of the associated mathematical fault inputs.
In particular, considering the possible faults affecting the spin rate sensors of the reaction wheels, it results that a generic j-th physical sensor fault F_{ω_j} $(j = 1, ..., 3)$ can be associated to three (*i.e.* $\nu_k = 3$) mathematical fault inputs $f_{\omega_{j,k}}$ $(k = 1, ..., \nu_k)$ and corresponding vector fields $\ell_{\omega_{j,k}}(x)$, where the fault inputs $f_{\omega_{j,3}}$ $(j = 1, ..., 3)$ correspond to the time derivatives $\dot{F}_{\omega_j} = (\dot{\omega}_{w_j} - \dot{\omega}_{w_{y,j}})$ of the physical sensor faults.
Finally, due to the possible presence of parametric uncertainties in the aerodynamic force model, the overall aerodynamic disturbance term to be decoupled can be defined through the (uncertain) aerodynamic force term $d = F_{aero}$ and the corresponding vector field $p(x)$. Therefore, if (1), (2) and (6) are rewritten by considering the outputs $\omega_{w_{y,j}} = \omega_{w_j} - F_{\omega_j}$ of the sensors as new state variables for the system dynamics, the general structure of (7) affine in both the disturbance, actuator and sensor fault inputs is recovered. Hence, the final nonlinear model, including the effects of all the (non-concurrent) faults affecting the actuators and sensors, can be written as follows:

$$\begin{aligned} \dot{y} = n(y) + p(y)\, d_{aero} + \sum_{i=1}^{3} g_i(y)\, M_{c,i} + \\ + \sum_{i=1}^{3} \ell_{M_i}(y)\, f_{M_i} + \sum_{j=1}^{3} \sum_{k=1}^{\nu_k} \ell_{\omega_{j,k}}(y)\, f_{\omega_{j,k}} \end{aligned} \tag{11}$$

This model of the faulty system, expressed as function of the available commanded inputs M_c and measured outputs y, results to be affine in all the control and (unknown) fault inputs. Therefore, any discrepancy between the fault-free and faulty system dynamics is completely modelled through the introduced fault inputs, and the NLGA can be exploited for the design of the aerodynamic decoupled FDI residual filters.

3.3 Design of the Fault Detection and Isolation Module

Starting from (8), a generic residual generator can be modelled in filter form as follows:

$$\begin{cases} \dot{\xi} = n_1(\bar{y}_1, \bar{y}_2) + g_1(\bar{y}_1, \bar{y}_2)\, u_c + L(\bar{y}_1 - \xi) \\ \varepsilon = \bar{y}_1 - \xi \end{cases} \tag{12}$$

where $L > 0$ is the gain of the residual filter such that the residual filter is asymptotically stable, and ε is the generated diagnostic signal. Moreover, proper scalar components $\bar{x}_{1s}$ of $\bar{x}_1$ which are affected by the fault term f can be extracted, and this scalar components can be exploited to design the mathematical models of scalar NLGA residual filters.
It is straightforward to design three simple NLGA residual filters, which exploit only the available flywheel spin rate measurements provided by the reaction wheel sensors, directly on the basis of (6). Each of these *local* NLGA residual filters results to be sensitive only to the couple of faults f_{M_i}, *i.e.* the actuator fault itself, and $f_{\omega_{i,3}} = \dot{F}_{\omega_j}$, *i.e.* the time derivative of the fault on the sensor related

to the same i-th reaction wheel. Moreover, these local filters are independent of the aerodynamic disturbance and satellite attitude. However, even if these local filters allow the isolation of the reaction wheel subsystem affected by a possible actuator or sensor fault, it is not possible to achieve an exact and complete fault isolation by exploiting only these local filters. Hence, the design of additional residual filters is required in order to classify a detected fault as an actuator or sensor fault.

The use of the NLGA allows to design six additional residual filters, on the basis of (1) and (2), which are decoupled from the aerodynamic disturbance in order to obtain residual filters not subject to detection errors due to parametric uncertainties of the aerodynamic disturbance model. Each of these designed *global* NLGA residual filters exploits also satellite attitude and angular speed measurements in addition to the local flywheel spin rate measurements. Each of these designed filters results to be sensitive to a different couple of possible actuator faults and to all the physical sensor faults through one or more associated mathematical fault inputs, generally with fault sensitivities depending on the satellite attitude. However, it is also possible to design residual filters presenting a constant fault sensitivity gain independent of the satellite attitude with respect to one of the two actuator faults and two of the introduced sensor fault inputs. On the other hand, the fault sensitivity gains related to the other actuator and introduced sensor fault inputs remain dependent on the satellite attitude.

Therefore, it is possible to design a bank of nine scalar NLGA disturbance decoupled filters derived from (1), (2) and (6), organised as a *generalised scheme*, consisting of the three local and six global residual filters. The scalar state variables ξ of the designed NLGA global and local residual filters are defined as follows:

$$\begin{array}{ll} \xi_{global_1} = J_{xx}\omega_1 - J_{yy}\omega_2 p_1/p_2 & \xi_{local_1} = \omega_{w_1} \\ \xi_{global_2} = J_{yy}\omega_2 - J_{xx}\omega_1 p_2/p_1 & \xi_{local_2} = \omega_{w_2} \\ \xi_{global_3} = J_{xx}\omega_1 - J_{zz}\omega_3 p_1/p_3 & \xi_{local_3} = \omega_{w_3} \\ \xi_{global_4} = J_{zz}\omega_3 - J_{xx}\omega_1 p_3/p_1 & \\ \xi_{global_5} = J_{yy}\omega_2 - J_{zz}\omega_3 p_2/p_3 & \\ \xi_{global_6} = J_{zz}\omega_3 - J_{yy}\omega_2 p_3/p_2 & \end{array} \tag{13}$$

where the terms $p_1(x)$, $p_2(x)$ and $p_3(x)$ are functions of the satellite attitude and position of the aerodynamic centre of pressure. The fault detection and isolation task is achieved by means of a proper residual cross-check procedure and exploiting a suitable decision logic to correctly detect and isolate the fault, with the assumption of multiple nonconcurrent faults.

Due to the presence of measurement noise, thresholds have to be properly selected for each generated residual signal in order to achieve the best performances in term of false alarm rate and missed fault rate. In practice, the value of these thresholds have been experimentally selected in the fault-free condition and for each residual signal separately.

4. FAULT DIAGNOSIS

4.1 Design of the Fault Estimation Module

The fault estimation module consists of six independent adaptive fault estimation filters, each of them responsible of providing the estimate of a specific fault affecting an actuated control torque or a flywheel spin rate measurement. These adaptive fault estimators are derived from the same $\bar{x}_{1s}$-subsystems exploited to design the models of the local residual filters, and exploit Radial Basis Function Neural Networks (RBF NNs) in order to accurately estimate an occurred generic fault.

For a sufficiently large number N of hidden-layers neurons and if the system state x takes on values in a compact set $X \subset \mathcal{R}^{\ell_n}$, a weight matrix W can be determined such that a generic continuous function $f(x)$ can be approximated by RBFs, with a guaranteed finite model error e^* (Castaldi et al. (2014)):

$$f(x) = W\varphi(x) + e(x) = \sum_{k=1}^{N} w_k \varphi_k(x) + e(x) \tag{14}$$

where W is an optimal *constant* weight matrix, φ_k is k-th radial basis function and $e(x)$ is the model approximation error satisfying $|e(x)| \leq e^*$. In this paper, the RBFs are assumed to be modelled as Gaussian functions as follows:

$$\varphi_k(\hat{x}) = \exp(-|\hat{x} - \mu_k|^2 \Big/ \sigma_k^2) \tag{15}$$

where μ_k and σ_k are the center and the width of the k-th radial basis function respectively. Considering the occurrence of possible actuator faults, the scalar model (12) of each local residual filter is modified, in order to design just as many RBF NN adaptive filters for torque fault estimation, as follows:

$$\begin{cases} \dot{\xi} = n_{1s}(\bar{y}_1, \bar{y}_2) + g_{1s}(\bar{y}_1, \bar{y}_2)\, u_c + \\ \qquad + \ell_{1s}(\bar{y}_1, \bar{y}_2)\, f + L(\bar{y}_{1s} - \xi) \\ \varepsilon = \bar{y}_{1s} - \xi \end{cases} \tag{16}$$

where the actuator torque fault function $f = F_{Mi}$ $(i = 1, ..., 3)$ is estimated by a RBF NN:

$$\hat{f} = \hat{F_{Mi}} = \hat{W}\varphi(\xi) \tag{17}$$

as shown in (14), with the weight matrix $\hat{W}$ determined by the following adaptive law:

$$\dot{\hat{W}} = \eta D \varepsilon \varphi^T(\xi) \tag{18}$$

where $\eta > 0$ is the learning ratio and D is a proper constant matrix such that the RBF NN adaptive filter (16) is asymptotically stable.

On the other hand, considering the occurrence of possible sensor faults, the model (12) of each of the three scalar NLGA local residual filters is modified in a slightly different manner, in order to design just as many RBF NN adaptive filters for sensor fault estimation, as follows:

$$\begin{cases} \dot{\xi} = n_{1s}(\bar{y}_1, \bar{y}_2) + g_{1s}(\bar{y}_1, \bar{y}_2)\, u_c + L(\bar{y}_{1s} - \xi) \\ \varepsilon = \bar{y}_{1s} - \xi - f \end{cases} \tag{19}$$

where the actuator torque fault function $f = F_{\omega j}$ $(j = 1, ..., 3)$ is estimated by a RBF NN:

$$\hat{f} = \hat{F_{\omega j}} = \hat{W}\varphi(\xi) \tag{20}$$

as shown in (14), with the weight matrix $\hat{W}$ determined by the same adaptive law of (18), where $\eta > 0$ is the learning ratio and D is a proper constant matrix such that the RBF NN adaptive filter (19) is asymptotically stable.

5. SIMULATION RESULTS

Some results achieved in Matlab/Simulink® are reported. The principal dimensions of the satellite body are $d = 0.6\,\mathrm{m}$, $w = 2\,\mathrm{m}$, and $h = 7.5\,\mathrm{m}$, $\mathbf{r_{cp}} = [0.10,\ 0.15,\ -0.35]\,\mathrm{m}$ is the aerodynamic torque displacement vector, while the inertia values are $I_{xx} = 330\,\mathrm{kg}\cdot\mathrm{m}^2$, $I_{yy} = 280\,\mathrm{kg}\cdot\mathrm{m}^2$, $I_{zz} = 60\,\mathrm{kg}\cdot\mathrm{m}^2$. A flywheel moment of inertia $J_w = 0.005\,\mathrm{kg}\cdot\mathrm{m}^2$ and initial flywheel spin rate values $\omega_0 = [3000, 3000, 3000]^T$ rpm for the three considered reaction wheels are considered.

A terrestrial mission with a circular orbit at an altitude of 350 km and null inclination, with a low Earth equatorial orbit radius $R = 6728.140\,\mathrm{km}$ is considered. The atmosphere density is $\rho = \rho_{max} = 6\cdot 10^{-11}\,\mathrm{kg/m^3}$, the drag coefficient is $C_D = 2.2$, and the orbital velocity is $V = 8187.63\,\mathrm{m/s}$, and μ is equal to the Earth's gravitational constant, $\mu = 39.86004418\cdot 10^{13}\,\mathrm{m^3/s^2}$.

Two types of additive faults are considered, commencing at $t_{fault} = 7.5\,\mathrm{s}$ and affecting the attitude control torque M_3 and the spin rate measurement ω_{w_3} of the third reaction wheel: an actuator fault $f_{M_3} = a_M\,\omega_{w_3}$ with size a_M passing from zero to $= 0.0025\,\mathrm{Nms}$ at $t = 12.5\,\mathrm{s}$ and a sensor fault $f_{w_3} = a_\omega\,\omega_{w_3}$ with $a_\omega = -0.005$. Both these types of faults are modelled as functions of the actual flywheel rotation speed (measured in rad/s). The first one can represent an increase of friction in the actuator motor due to lubrication problems or damages in the actuator bearing unit. The second one can represent a reduced pulse count caused by the obstruction of some slits of the code disk of the optical encoder of the actuator.

Sensor noises are modelled by Gaussian processes with zero mean. Standard deviations equal to 3 arcsec, 3 arcsec/s and 1 rpm are assumed for the attitude measured in Euler angles, satellite angular speed and flywheel spin rate measurements, respectively. $N = 41$ Gaussian RBFs have been considered, with width $\sigma_k = 5$ and centers μ_k equally spaced between -40 and $40\,\mathrm{kg\ m^2}$. A simulation time of 30 s with a sampling time of 0.01 s is considered.

Considering the occurrence of the actuator fault, Fig. 1 shows the diagnostic signals provided by the NLGA local residual filters. The third subplot depicts the residual sensitive to the couple of faults $f_{M_3}, f_{\omega_{3,3}}$, with unitary gain and independent of the aerodynamic disturbance and satellite attitude. On the other hand, the first and second subplots show the local residuals sensitive only to $f_{M_1}, f_{\omega_{1,3}}$ and $f_{M_2}, f_{\omega_{2,3}}$, respectively. The selected thresholds are depicted for each residual by means of red lines. Since each local residual is sensitive only to actuator and sensor faults occurring on a specific reaction wheel subsystem, it is possible to detect and isolate the faulty subsystem just by means of the local residuals. However, the global residuals must be exploited if the precise fault isolation is needed.

Fig. 2 show the diagnostic signals provided by the two NLGA global residual filters sensitive to the actuator fault f_{M_3} with selected constant gain, decoupled from the aerodynamic disturbance and independent of the satellite attitude. As shown, both of them exceed the selected thresholds after the fault occurrence. On the other hand, Fig. 3 represents the two global residuals not sensitive to the actuator fault f_{M_3} in any satellite attitude condition, which remain between the selected threshold values. In order to clearly illustrate how the precise fault isolation can be achieved by exploiting the global residuals, the occurrence of the sensor fault can be considered and the behaviour of the obtained diagnostic signals can be compared. Fig. 4 shows the residual provided by the third NLGA local residual filters in case of sensor fault occurrence. This residual results to be the only one sensitive to the occurred fault as in the previous case. Fig. 5 depicts the diagnostic signals provided by the two NLGA global residual filters sensitive to the actuator fault f_{M_3} with constant gain, decoupled from the aerodynamic disturbance and independent of the satellite attitude. Again, both of them exceed the selected thresholds after the fault occurrence. On the other hand, Fig. 6 shows the two global residuals that are not sensitive to the actuator fault f_{M_3} and sensitive only to f_{M_1} and f_{M_2}, respectively with selected constant gain with respect to a specific actuator fault of these two. Since both these global residuals exceed their thresholds, although this should not happen in case

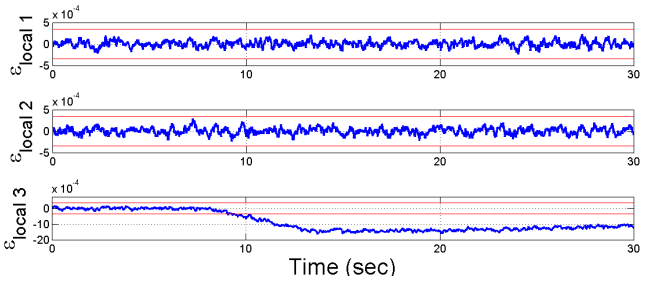

Fig. 1. Actuator fault scenario: decoupled local residuals, each being sensitive to faults on a specific reaction wheel.

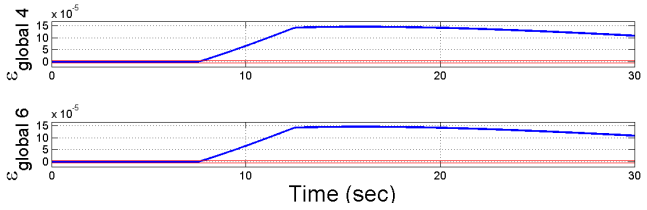

Fig. 2. Actuator fault scenario: decoupled global residuals sensitive to the actuator fault f_{M_3} with constant gain.

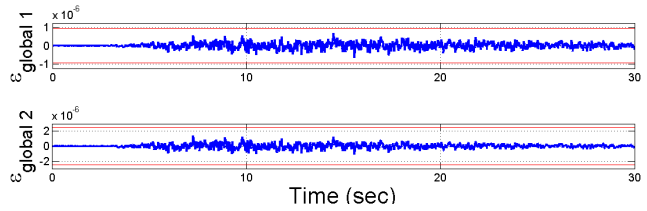

Fig. 3. Actuator fault scenario: decoupled global residuals not sensitive to the actuator fault f_{M_3}.

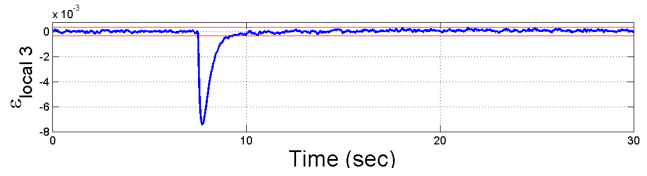

Fig. 4. Sensor fault scenario: decoupled local residual sensitive to faults on the third reaction wheel.

the actuator fault f_{M_3} occurs, it results that a sensor fault in the third reaction wheel subsystem must be occurred in this case due to the assumption of single fault. Hence, thanks to the different behaviour of the global residuals in the two fault cases, the occurrence of the the actuator fault can be recognized and isolated in the first case, and the occurrence of the sensor fault in the second one. Once the occurred fault is detected and correctly isolated, the corresponding adaptive estimation filter is activated.

Finally, Figs. 7 and 8 show the fault estimates obtained

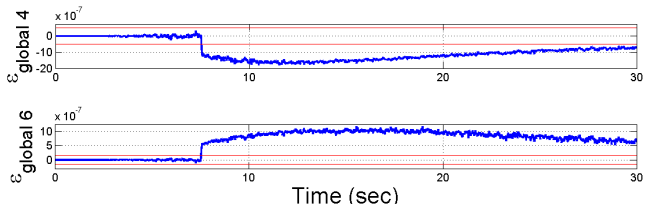

Fig. 5. Sensor fault scenario: decoupled global residuals sensitive to the actuator fault f_{M_3} with constant gain.

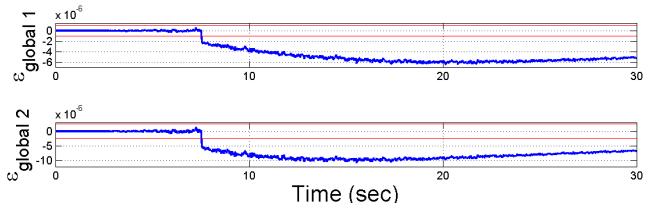

Fig. 6. Sensor fault scenario: decoupled global residuals not sensitive to the actuator fault f_{M_3}.

once the actuator fault F_{M_3} and sensor fault F_{ω_3} have been isolated and the proper NLGA RBF NN adaptive estimation filters activated, respectively. It can be seen that the adaptive filters provide accurate actuator and sensor fault estimates, even in case of generic fault functions.

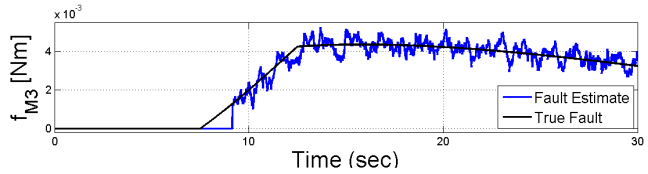

Fig. 7. Estimate of the actuator fault F_{M_3}.

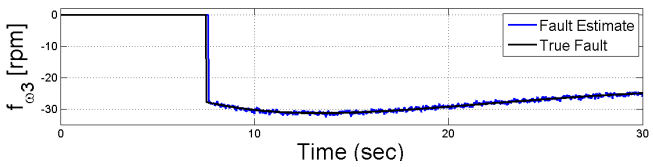

Fig. 8. Estimate of the physical sensor fault F_{ω_3}.

6. CONCLUSION

This paper presented a novel Fault Detection and Diagnosis scheme for the diagnosis of actuator and sensor faults affecting the reaction wheel subsystems of a Low Earth Orbit satellite. The designed diagnosis system exploits both local flywheel spin rate measurements and global satellite attitude and angular speed measurements in order to obtain a precise fault detection and isolation. Due to the aerodynamic parameter uncertainty, the disturbance decoupling achieved thanks to the NonLinear Geometric Approach allows to obtain better fault detection and isolation performances. Moreover, the use of Radial Basis Function Neural Networks allows designing generalised fault estimation filters, able to estimate a generic fault function without needing any a priori information about the fault internal model. The given simulation results highlight that the proposed diagnosis system can achieve a precise fault detection and isolation and provide accurate fault estimates independent of the aerodynamic disturbance.

REFERENCES

Baldi, P., Castaldi, P., Mimmo, N., and Simani, S. (2013). Satellite attitude active FTC based on geometric approach and RBF neural network. *2013 Conference on Control and Fault Tolerant Systems*, Nice (France).

Blanke, M., Kinnaert, M., Lunze, J., and Staroswiecki, M. (2006). *Diagnosis and fault–tolerant control*. Springer–Verlag, Berlin (Germany).

Bokor, J. and Szabó, Z. (2009). Fault detection and isolation in nonlinear systems. *Annual Reviews in Control*, 33, 113–123.

Calhoun, P.C., and Garrick, J.C. (2007). Observing mode attitude controller for the lunar reconnaissance orbiter. *20–th International Symposium on Space Flight Dynamics*, Annapolis (MD).

Castaldi, P., Mimmo, N., Naldi, R. and Marconi, L. (2014). Robust trajectory tracking for underactuated VTOL aerial vehicles: Extended for adaptive disturbance compensation. *Proc. of 19–th IFAC World Congress, 2014*, 19(1), 3184–3189.

De Persis, C., and Isidori, A. (2001). A geometric approach to nonlinear fault detection and isolation. *IEEE Trans. on Automatic Control*, 45, 853–865.

Ding, S.X. (2008). *Model–based fault diagnosis techniques: Design schemes, algorithms, and tools*. Berlin Heidelberg: Springer.

Edelmayer, A., Bokor, J., Szabó, Z. and Szigeti, F. (2004). Input reconstruction by means of system inversion: A geometric approach to fault detection and isolation in nonlinear systems. *International Journal of Applied Mathematics and Computer Science*, 14(2), 189–199.

Isermann, R. (2006). *Fault diagnosis systems: An introduction from fault detection to fault tolerance*. Springer–Verlag.

Lorentzen, T., Blanke, M. and Niemann, H.H. (2003). Structural analysis – A case study of the Rømer satellite. *Proc. of IFAC Symp. Safeprocess 2003*, Elsevier – IFAC.

Mattone, R., and De Luca, A. (2006). Nonlinear fault detection and isolation in a three–tank heating system. *IEEE Trans. on Control Systems Technology*, 14(6), 1158–1166.

Sobhani–Tehrani, E., Talebi, H.A., and Khorasani, K. (2014). Hybrid fault diagnosis of nonlinear systems using neural parameter estimators. *Neural Networks*, 50, 12–32.

Wie, B. (2008). *Space vehicle dynamics and control* (2nd ed.). AIAA Education Series.